Supplementary Material: An isotropic model for cluster growth on a regular lattice

Christian A. Yates and Ruth E. Baker

Centre for Mathematical Biology, Mathematical Institute, University of Oxford, 24-29 St Giles', Oxford OX1 3LB, UK[*]

(Dated: June 11, 2013)

PACS numbers: 61.46.Bc, 89.75.Da, 68.35.Ct, 81.05.Xj, 36.40.Mr, 87.18.Hf, 87.18.Ed,

[*]yatesc@maths.ox.ac.uk; http://people.maths.ox.ac.uk/yatesc/

I. ANISOTROPY OF THE EDEN MODEL

We measured the anisotropy of Eden clusters using our bespoke anisotropy metric and found good agreement with the values found by Batchelor and Henry [3] of $\sim +2\%$ in the axial directions and $\sim -2\%$ in the diagonal direction (see Fig. 1). These results verify the consistency of our choice of anisotropy metric.

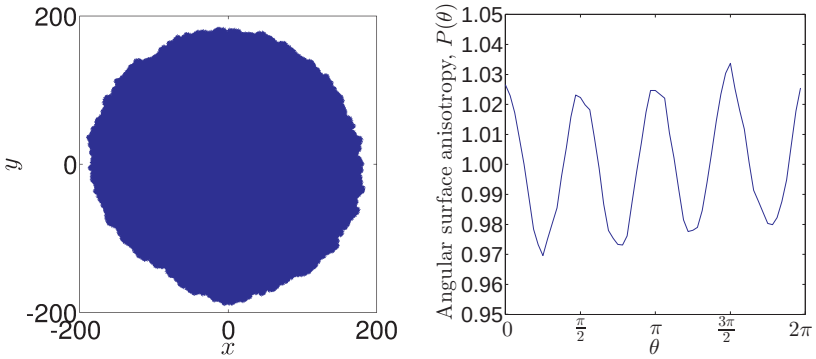

(a) (b)

FIG. 1. *The anisotropy of Eden clusters. (a) A typical example of an Eden C cluster displaying slightly flatter edges in the diagonal directions. (b) The angular surface anisotropy, $P(\theta)$. Clear axial anisotropy of the clusters is observed in our measure. Clusters were grown to $N = 10^5$ elements and anisotropy values are averaged over 200 repeats.*

II. NOISE REDUCTION

Noise reduction is a technique which is used to reduce the influence of finite-size effects on the behavior of large clusters. New surface-addition sites are selected as usual, but instead of filling a selected site with an element, a counter associated with that site is incremented by one. Only when the counter for a site reaches the 'noise reduction parameter', m, is an element added to that site. The growth rate of clusters in specific areas is, therefore, reduced and growth is spread more evenly across the surface. Noise reduction can be thought of as playing a similar role to surface tension, smoothing surfaces by removing many of the holes and overhangs responsible for the intrinsic width of the surface [8]. The waiting time distribution at each site becomes more peaked as m increases and the variance decreases. If, in the non-noise-reduced model, element addition can be considered to be a Poisson process,

then waiting times will be exponentially distributed:

$$p(t) = \lambda e^{-\lambda t} \quad \text{for } t \geq 0,$$

where $\lambda > 0$ is the reciprocal of the expected waiting time or 'rate parameter'. The waiting time for the m^{th} occurrence of an exponentially distributed random variable is Erlang[1] distributed:

$$p(t) = \frac{\lambda^m t^{m-1} e^{-\lambda t}}{(m-1)!} \quad \text{for } t \geq 0.$$

We set the rate parameter $\lambda = m$ so that the mean waiting time, λ/m, remains unchanged. The larger the value of m (known as the 'shape parameter'), the more sharply peaked the Erlang distribution becomes (see Fig. 2 (a)). In the noise-reduced limit, $m \to \infty$, the waiting times become δ-distributed and the model becomes deterministic. Therefore, in the Eden model, all available surface sites are filled at exactly the same time. In this limit, it is easy to see that clusters are built up by the simultaneous addition of layers of elements, one layer at a time. This leads to diamond shaped Eden clusters in two dimensions or octahedral shaped clusters in three dimensions, clearly exposing the anisotropic nature of the on-lattice Eden model (see Fig. 2 (b)).

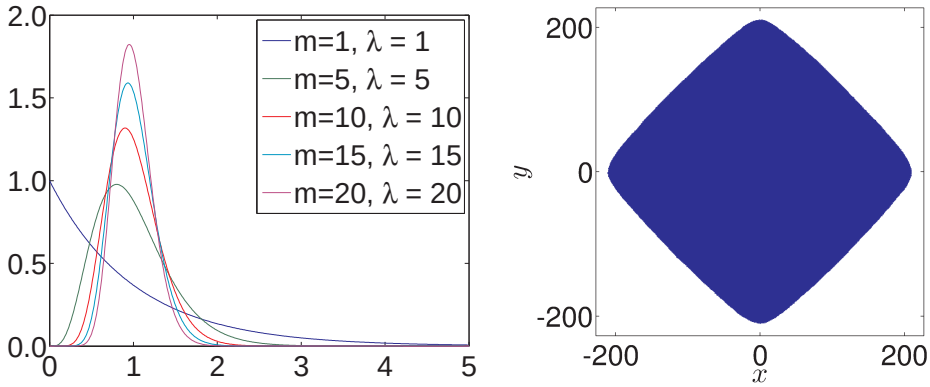

(a) (b)

FIG. 2. *The noise-reduced Eden model. (a) The Erlang distribution becomes more and more peaked as the shape parameter (i.e. the noise reduction parameter), m, and the rate parameter, $\lambda(= m)$, increase. (b) A typical noise-reduced ($m = 60$) Eden C cluster ($N = 10^5$ elements). The underlying axial anisotropy is clearly evident.*

III. ANISOTROPY METRIC TESTS

In order to examine our anisotropy metric and to determine whether it is influenced by the square lattice, we tested it on a series of artificial clusters: the circle, the square and the diamond (see Figs. 3 (a), (b) and (c), respectively). We made these test clusters representative of the size of cluster we will be simulating (i.e. $\sim 10^5 - 10^6$ elements).

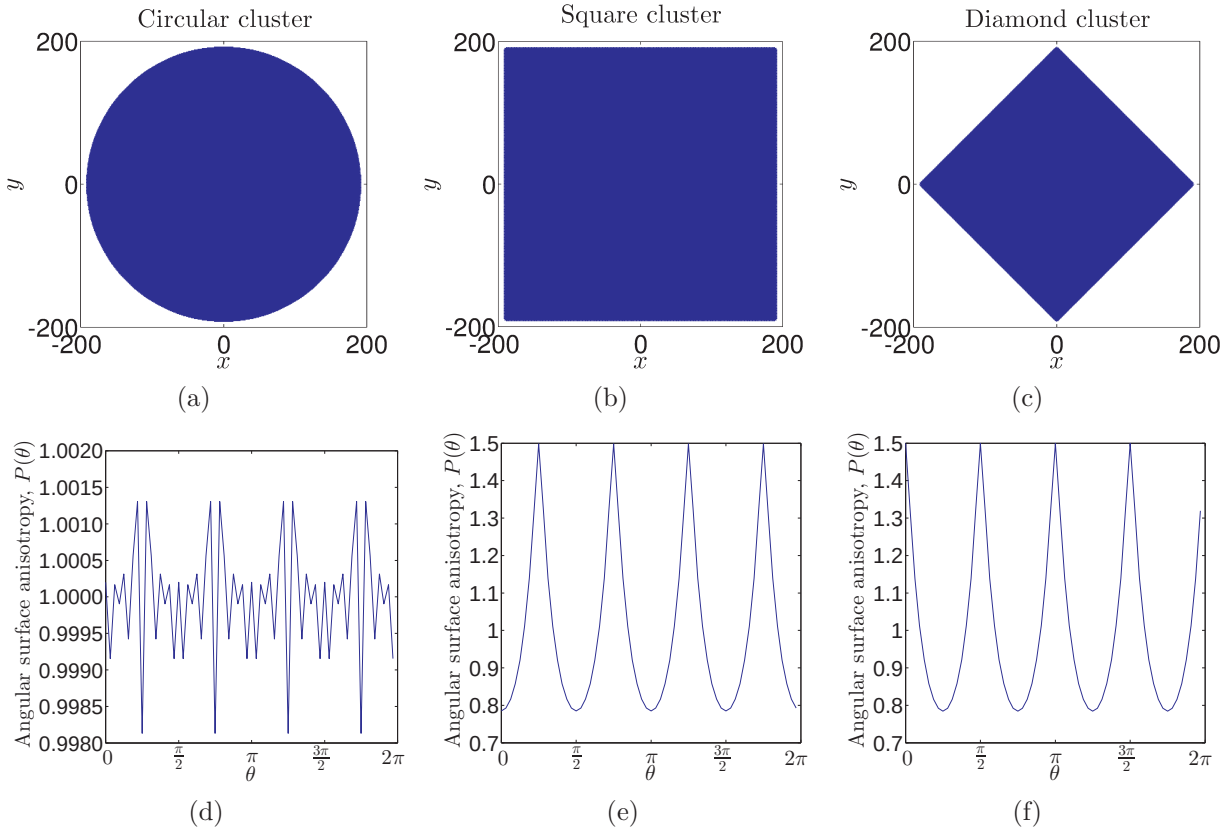

FIG. 3. *Determining the effectiveness of the anisotropy measure on some sample clusters. The angular surface anisotropy measure, $P(\theta)$, ((d), (e) and (f)) is able to detect strongly isotropic clusters such as the square ((b) $N = 143641$) and the diamond ((c) $N = 71821$). The metric gives relatively constant values of anisotropy (in comparison to the oscillating values for the square and diamond clusters) for the circular cluster ((a) $N = 112825$), but a small amount of anisotropy is inherent (note the different scales on the x-axis in (e) and (f) in comparison to (d)). This anisotropy decreases the larger the cluster size (data not shown).*

Our measure of anisotropy, introduced in the main text, discerns the strong diagonal anisotropy in the square cluster and the axial anisotropy in the diamond cluster (see Fig. 3). The maximum anisotropy of the angular surface anisotropy measure, $P(\theta)$, when applied to the circular cluster is around 0.2%. We bear this in mind when drawing conclusions about the isotropy or otherwise of clusters.

IV. FOURIER DECOMPOSITION FOR DETERMINING ANISOTROPY

In this section we present the results alluded to in the main text which examine our eye-balled assertions about the isotropy or otherwise of the various clusters. We implement a Fourier decomposition of the angular surface anisotropy measure, $P(\theta)$, in order to ascertain which modes contribute most significantly and consequently the relative sizes of the anisotropies of each cluster in the corresponding directions.

A. Test clusters

We begin by analysing the test clusters presented in the previous section in order to give the reader an intuition regarding the expected pattern of the Fourier coefficients for general clusters by considering the pattern for these three characteristic clusters.

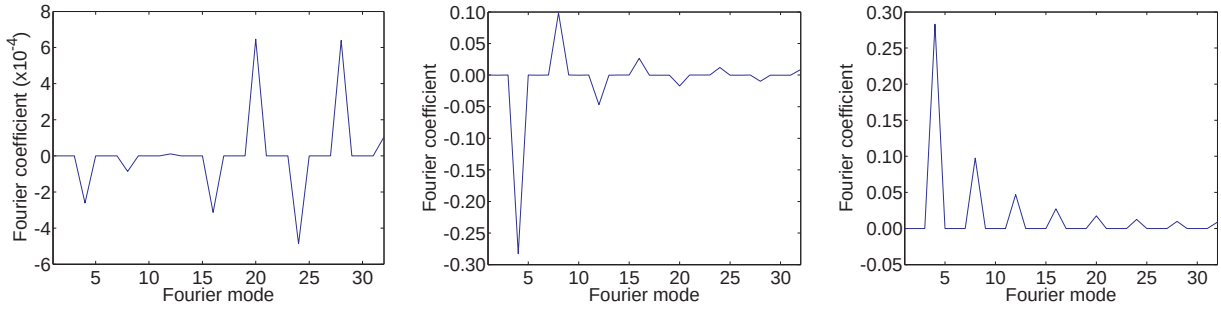

(a) (b) (c)

FIG. 4. *The Fourier coefficients of $P(\theta)$ for the three characteristic clusters ((a) circle, (b) square and (c) diamond) presented in the previous section. Note the drastically different scales on the axes.*

The circular cluster exhibits very small Fourier coefficients (see Fig. 4 (a)) indicative of its isotropic nature. The square cluster, on the other hand, exhibits some large Fourier coefficients (See Fig. 4 (b)). In particular the quadrupole (corresponding to the fourth Fourier coefficient) is negative with large magnitude and the eighth is also large, but positive. This is indicative of the strong negative axial and positive diagonal anisotropies associated with the square cluster. The $4n^{th}$ Fourier coefficients (for integer n) are significantly different from zero and follow the alternating sign pattern of the fourth and eighth coefficients. The magnitudes of these later coefficient decrease monotonically with increasing n indicating that these contributions to the overall shape of the cluster are less significant. Finally the

Fourier spectrum of the diamond (see Fig. 4 (c)) also has significant positive contributions from every 4th multipole which decrease in magnitude as the order of the multipole increases. The dominant contributions is from the quadrupole, indicating a strong positive axial anisotropy, but interestingly the octupole (corresponding to the eighth Fourier coefficient) is also positive. In the absence of a large quadrupole we might take this as evidence for a positive diagonal anisotropy, but clearly the contribution from the quadrupole has a more significant effect on the shape of the cluster.

B. The 'isotropic' Eden C model

In order to assess the anisotropy of noise-reduced clusters grown with the 'isotropic' Eden C model of Paiva and Ferreira Jr [7] we carry out the Fourier decomposition of $P(\theta)$ as given in Fig. 2 (c) of the main text. The large negative value of the fourth Fourier coefficient

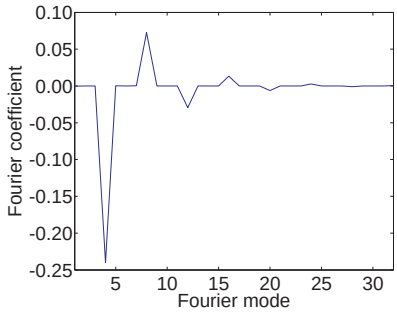

(a)

FIG. 5. *The Fourier coefficients of $P(\theta)$ for the 'isotropic' Eden C model of Paiva and Ferreira Jr [7].*

and the large positive value of the eighth Fourier coefficient (see Fig. 5) are consistent with the negative axial and positive diagonal anisotropies surmised from Fig. 2 (c) of the main text. In addition, it is clear that every fourth multipole has a contribution to the isotropy, although the magnitude of these contributions decreases sharply as the order of the multipole increases, implying less significance for the higher order multipoles. This behaviour is reminiscent of that described for the square cluster in the previous subsection and is indicative of the square nature of the clusters formed using this model.

C. The Drasdo model

We carry out the same analysis for $P(\theta)$ ascertained from clusters grown according to the model of Drasdo [5] as given in Fig. 3 (b) of the main text. The large negative value of

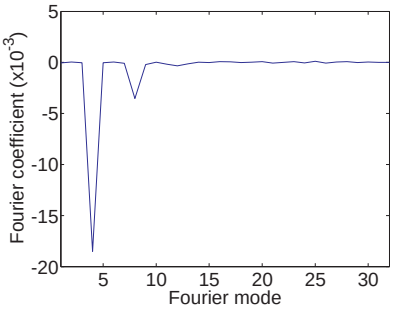

(a)

FIG. 6. *The Fourier coefficients of $P(\theta)$ for the model of Drasdo [5].*

the fourth Fourier coefficient is consistent with the negative axial anisotropy surmised from Fig. 3 (b) of the main text. Interestingly the octupole is also negative (but with smaller magnitude than the quadrupole). In the absence of the large negative quadrupole this might lead us to suggest a negative diagonal anisotropy, however, the octupole also contributes to the surface in the axial directions so in combination with the large negative quadrupole we can make sense of the apparent positive axial anisotropy evident in Fig. 3 (b) of the main text.

D. The model of Ferreira and Alves

Finally we employ the Fourier decomposition on $P(\theta)$ ascertained from noisy and noise-reduced clusters grown according to the model of Ferreira Jr. and Alves [6] as given in Fig. 5 (a) and (b), respectively, of the main text. For the noisy cluster (see Fig. 7 (b)) the finite size effects associated with its growth tend to mask any anisotropy that may be underlying the model although we still see a relatively large positive contribution from the quadrupole indicating a slight axial anisotropy. This is confirmed in the noise-reduced version of the model (see Fig. 7 (b)). The positive quadrupole and negative octupole are indicative of a slight axial anisotropy. However, we note the scale of the y-axis in comparison to those of previous models: the magnitude of the dominant Fourier coefficient for the noise-reduced

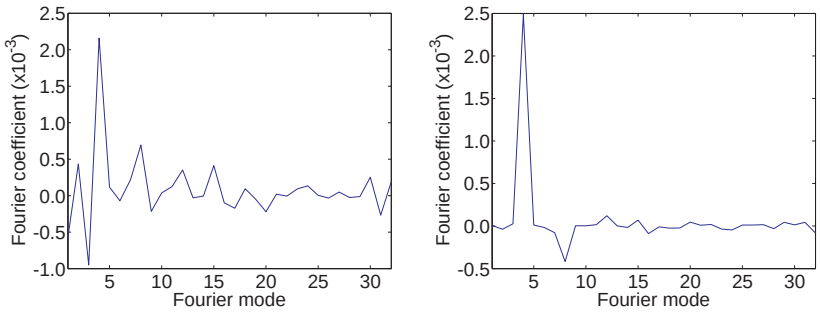

(a) (b)

FIG. 7. *The Fourier coefficients of $P(\theta)$ for both the noisy and noise-reduced versions of the model of Ferreira Jr. and Alves [6].*

version of the model of Ferreira Jr. and Alves [6] (see Fig. 7 (b)) is almost an order of magnitude smaller than that of the that of the dominant Fourier coefficient for the model of Drasdo [5] (see Fig. 6 (a)) and only around 3 times as large as dominant Fourier coefficient of the truly circular cluster (see Fig. 4 (a)) making the model of Ferreira Jr. and Alves [6] the least anisotropic on-lattice growth model currently available.

V. SCALING OF THE EDEN MODEL

Fig. 8 (a) shows for '1+1' dimensional, strip simulations the increase of the surface width of the Eden model over time for a variety of different substrate lengths ($l = 10, 20, 40, 80$) on a log-log plot. The dependence of the surface width on the 'effective height', $\hat{h}$, for each value of l, has two well-demarcated regions separated by a crossover height, which we will denote h_+ (see Fig. 8 (b)). Although this crossover point occurs at different values of $\hat{h}$ for each different substrate length it is clear that the width of the interface increases initially as a power-law in effective height:

$$w(l, \hat{h}) \sim \hat{h}^{\beta} \qquad \text{when} \qquad \hat{h} \ll h_+. \tag{1}$$

The exponent β is known as the growth exponent and characterizes the dynamical behavior of the roughening process [2].

Eventually, due to surface correlations, the width of the surface reaches capacity for the given substrate length and the variation of the surface width with the effective height levels off (see the horizontal regions of Fig. 8 (a)). However, the value of the interface width

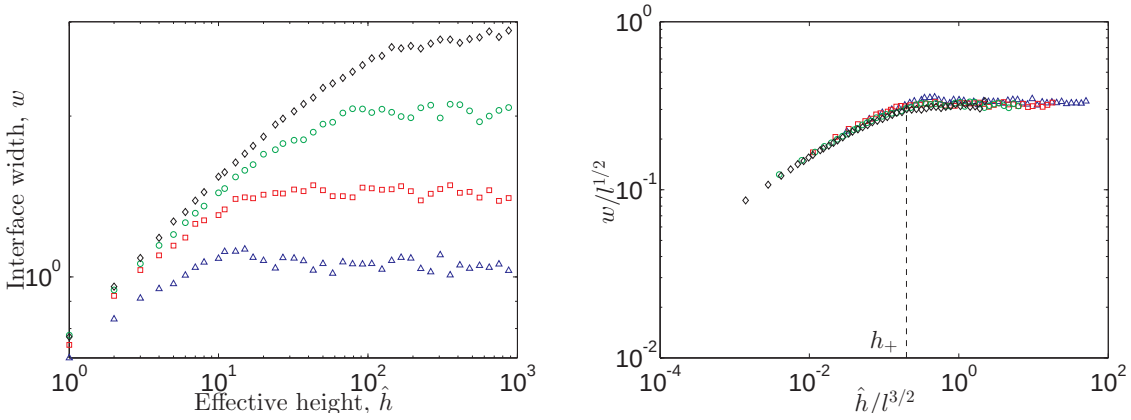

FIG. 8. *The evolution of the surface width for the Eden C model for different system sizes. (a) The logarithmic scale displays the clear initial power law dependence of surface width on effective height and the eventual saturation of surface width to the value $w_{cap}(l)$ (see equation* (2)*). (b) The evolution of surface width rescaled according to the Family-Vicsek relationship (equation* (3) *of the main text). The functional form of the scaling function $f(x)$ and its properties in different regimes, as described in equation* (3) *of the main text, are clearly evident. The scaled crossover height, h_+, is marked as a vertical, black, dashed line. In both sub-figures blue triangles (△) correspond to system size $l = 10$, red squares (□) to $l = 20$, green circles (○) to $l = 40$ and black diamonds (◇) to $l = 80$.*

capacity, w_{cap}, is evidently dependent on the length of the substrate, l, (as the surface correlations take longer to spread across a wider surface). This dependence also follows a power law,

$$w_{\text{cap}}(l) \sim l^{\alpha} \qquad \text{when} \qquad \hat{h} \gg h_+. \tag{2}$$

This can be seen anecdotally from the roughly even spacing of the values of w_{cap} (on a log scale) for successively doubling substrate widths in Fig. 8 (a). The exponent α is known as the roughness exponent since it determines the maximum roughness of the interface.

The fact that surface width saturates at all is a combination of the effects of surface correlations and a 'finite size effect'. Surface correlations imply that, due to the nature of the particle addition process, the height of one column is affected by the heights of its neighboring columns. As the number of particles deposited increases, the distance over which these local correlations occur (the *correlation length*) increases until it is the same size as the substrate length and the correlations have, therefore, become global. At this point the surface width ceases to increase and has reached capacity. The finite size effect captures the idea that over an infinite substrate the correlations take an infinite amount of

time to become global and hence the surface would not saturate. Indeed it is only because the substrate has a *finite size* that we see saturation [2].

VI. THE HISTOGRAM DISTANCE ERROR METRIC

The Histogram distance error (HDE) between two surfaces (defined at discrete points), having normalized frequencies a_i and b_i at point i (i.e. $\sum a_i = \sum b_i = 1$), is given by

$$HDE = \frac{1}{2}\sum_{i=1}^{k} |a_i - b_i|, \tag{3}$$

where the sum is over all i such that either $a_i \neq 0$ or $b_i \neq 0$ [4]. In order to compare the particle densities for the discrete individual-based model and the continuum model, in the main text, we interpolate to find the value of the continuum solution surface at the centre of each of the interval in the individual based model. This provides us with two discrete solution surfaces which we can then compare using the HDE.

---

[1] The Erlang distribution is the discrete analogue of the gamma distribution.

[2] A.L. Barabási and H.E. Stanley. *Fractal Concepts in Surface Growth.* Cambridge University Press, 1995.

[3] M.T. Batchelor and B.I. Henry. Limits to Eden growth in two and three dimensions. *Phys. Lett. A*, 157(4-5):229–236, 1991.

[4] Y. Cao and L. Petzold. Accuracy limitations and the measurement of errors in the stochastic simulation of chemically reacting systems. *J. Comput. Phys.*, 212(1):6–24, 2005.

[5] D. Drasdo. Coarse graining in simulated cell populations. *Adv. Complex. Syst.*, 8(3):319, 2005.

[6] S.C. Ferreira Jr. and S.G. Alves. Pitfalls in the determination of the universality class of radial clusters. *J. Stat. Mech.-Theory. E.*, 2006(11):P11007, 2006.

[7] L.R. Paiva and S.C. Ferreira Jr. Universality class of isotropic on-lattice Eden clusters. *J. Phys. A.-Math. Theor.*, 40(1):F43–F49, 2007.

[8] T. Vicsek. *Fractal Growth Phenomena.* World Scientific, Singapore, 1992.